communications chemistry

A Nature Portfolio journal

Article

https://doi.org/10.1038/s42004-026-02165-6

Liquid-liquid phase-separated tau colocalizes with and stabilizes Aβ oligomers

Tina Jacob [1], Marie P. Schützmann [1], Laurin Gerhards[2], Laura Hruby[3], Gabriel Leprivier [3], Gültekin Tamgüney[1,2] & Wolfgang Hoyer [1,4]

Protein aggregation is a hallmark of neurodegenerative diseases, where misfolded proteins accumulate into insoluble deposits. Emerging studies indicate that liquid-liquid phase separation (LLPS) may serve as a transient stage in the transition from monomers to amyloid fibrils for several proteins implicated in neurological disorders. In this study, we investigated the interplay between tau and off-pathway oligomers of amyloid-beta (Aβ), the two key proteins in Alzheimer's disease (AD). Our findings demonstrate that tau condensates act as reservoirs for Aβ oligomers under LLPS conditions. Inside the tau condensates, Aβ oligomers reduced tau dynamics and formed discrete puncta, indicating a conducive environment for Aβ oligomer clustering. In contrast, in the absence of LLPS conditions, tau and Aβ oligomers formed solid-like co-aggregates with distinct morphologies. Tau significantly affected the kinetics of Aβ assembly, stabilizing off-pathway oligomers and inhibiting their replacement by amyloid fibrils. Our results highlight interactions between higher-order assemblies of tau and Aβ that may contribute to AD pathology.

Neurodegenerative diseases are characterized by the progressive loss of neurons, ultimately leading to cognitive impairment, and often involve protein misfolding and aggregation. Tauopathies are a subset of neurodegenerative diseases associated with the abnormal accumulation of tau protein[1]. Alzheimer's disease (AD) is the most prevalent tauopathy, characterized by the deposition of tau as neurofibrillary tangles (NFTs)[2]. Human tau is primarily expressed in neurons and associated with stability and organisation of microtubules by coordinating tubulin polymerisation[3,4]. At physiological conditions, tau remains stable across a wide range of pH, temperatures and ionic strengths, however at pathological conditions tau undergoes aggregation and deposits into insoluble amyloid fibrils. Tau lacks a well-defined three-dimensional structure and its disordered nature makes it highly prone to misfolding and aggregation[5]. The process of tau aggregation is progressive, initiating with smaller assemblies that gradually evolve into larger fibrils. This progression can be disease-specific with different tauopathies exhibiting distinct structural conformations, reflected in the unique folds adopted by tau in each disease[6].

Tau was recently identified to undergo liquid-liquid phase separation (LLPS), a process in which a homogeneous protein solution de-mixes into a dense protein-rich phase with distinct physicochemical properties. Tau forms highly concentrated protein condensates or droplets with liquid characteristics[7,8]. Phase separation of tau into these compartments leads to increased protein concentrations on a subcellular level which facilitates enhanced biochemical reaction rates. Studies on these tau condensates showed that upon prolonged maturation they can give rise to potential pathological conformations of tau and hence they may represent one of the initial stages of tau aggregation[9,10]. The evidence of in vivo tau condensates and their subsequent maturation into amyloid-like aggregates reinforces the important role of phase separation in tau aggregation[10]. Beyond the pathological roles, tau condensates also serve physiological functions, such as providing nucleation sites for tubulin polymerization, thereby facilitating microtubule assembly[11]. Phase separation is triggered when the concentration of the protein exceeds a certain threshold, and for tau this threshold is usually lowered by RNA or RNA-binding proteins[12] or by crowding agents[11,13]. This property of phase separation mirrors the need for heparin or other polyanions to induce tau aggregation in vitro[14], although the timescale of both processes can be variant, with LLPS happening within minutes while aggregation can take days.

Along with tau, the second polypeptide critically implicated in AD pathogenesis is amyloid-β (Aβ), which denominates mainly two peptides,

[1]Institut für Physikalische Biologie, Faculty of Mathematics and Natural Sciences, Heinrich Heine University Düsseldorf, Düsseldorf, Germany. [2]Institut für Biologische Informationsprozesse, Strukturbiochemie (IBI-7), Forschungszentrum Jülich GmbH, Jülich, Germany. [3]Institute of Neuropathology, University Hospital Düsseldorf and Medical Faculty, Heinrich Heine University, Düsseldorf, Germany. [4]Institute of Biological Information Processing (IBI-7: Structural Biochemistry), Forschungszentrum Jülich, Jülich, Germany. e-mail: wolfgang.hoyer@hhu.de

Aβ40 and Aβ42, resulting from the cleavage of amyloid precursor protein (APP) by γ-secretase[15]. Like tau, Aβ has no fixed secondary structure, and unlike tau, which needs either seeds or cofactors such as heparin for efficient aggregation, Aβ is highly aggregation-prone, forming β-sheet-rich structures which range from oligomeric species to amyloid fibrils and plaques which can also be found in AD brains. Unlike NFT spreading, however, the Aβ plaque load does not necessarily allow inference of the progression of symptoms, fitting to the hypothesis that the most aggressive form of Aβ are small soluble oligomers, not the mature amyloid fibrils[16,17].

Oligomers are metastable, pathological protein assemblies that adopt a morphology distinct from fibrils and arise during early stages of the assembly pathways. Membrane disruption, ion dysregulation, neuronal apoptosis, and neural signal dysfunction are some of the toxic effects of Aβ oligomers, leading to severe cognitive deficits. In addition, their ability to disrupt Ca^{2+} homeostasis[18] and to induce endoplasmic reticulum (ER) stress[19] makes them central to the progression of AD. The on-pathway and off-pathway models are two mechanisms depicting the observed diversity of oligomer formation[20,21]. On-pathway oligomers are transient pre-cursors of amyloid fibrils. In contrast, off-pathway oligomers are metastable, alternative aggregates that do not progress towards amyloid fibril formation, but have been linked to particularly detrimental activities[17,20,22].

Locating the primary pathological species among the many reported forms of tau and Aβ, including oligomers, condensates and fibrils, remains challenging[15,23] (Fig. 1). Rather than a single toxic conformer, it appears that a collective effect of these species underlies the pathology of neurodegenerative diseases[23]. The concurrent existence of NFTs and amyloid plaques in AD stresses that exploring the interplay between tau and Aβ is vital. Studies to date implicate the tau-Aβ interaction to be bi-directional where Aβ promotes the hyperphosphorylation[24] and causes missorting of tau[22] in cells, and reducing tau levels correlate with reduced Aβ toxicity[25,26]. With this evidence that AD is likely to result from an interplay between both tau and Aβ[27,28], understanding their early pathological assemblies and interactions could yield critical insights into the mechanisms driving AD pathology and progression[29–33]. Here, we investigate the interplay of off-pathway Aβ oligomers and tau, with a focus on LLPS conditions.

Results

Interaction of tau condensates with Aβ42 oligomers

The propensity of full-length 4R-Tau (hTau40; hereafter referred to as tau) to form condensates was studied at a tau concentration of 10 μM in Tris buffer (pH 7.4), in the presence of 10% polyethylene glycol (PEG 6000) as a molecular crowding agent. The presence of condensates was confirmed using differential interference contrast (DIC) microscopy and validated by confocal microscopy upon labelling tau with Alexa-647 fluorophore (Fig. 2A, B). The microscopy images support the phase separation ability of tau in vitro.

To study the interaction between Aβ oligomers and tau under LLPS conditions, tau condensates were incubated with Aβ42 oligomers (Aβ42Os). The critical oligomeric concentration (COC) represents the minimum monomer concentration above which the formation of metastable globular oligomers becomes thermodynamically favourable under the given solution conditions[34,35]. For Aβ42, the COC lies between 10 and 30 μM[36]; therefore, experiments were performed using oligomers derived from 40 μM Aβ42 (Fig. 3A).

We observed an interesting co-localisation of Aβ42O with tau condensates (Fig. 3B). The condensates were spherical and dynamic, consistent with a liquid-like nature (Supplementary Movies 1, 2). While tau remained homogeneously distributed within the condensates, Aβ42O displayed a non-uniform distribution, indicative of a multiphasic internal organization. The tau-Aβ42O co-condensates coexisted with amorphous aggregates harbouring both proteins (Fig. 3C). In contrast to the liquid-like condensates, these aggregates were immobile, consistent with solid-like properties, and exhibited substantial heterogeneity in size and morphology (Fig. 3C, Suppl. Movies 1, 2).

DimAβOs colocalize with tau condensates

Standard preparations of Aβ42Os typically contain considerable amounts of Aβ42 monomers and amyloid fibrils, due to the relatively high COC and the limited kinetic separation of oligomer and fibril formation phases[36]. In order to specifically investigate the interaction of tau with off-pathway oligomers of Aβ, we employed the dimeric Aβ variant termed dimAβ[35,36]. DimAβ mimics a high local concentration of Aβ by incorporating two covalently linked Aβ40 subunits in a single polypeptide chain, linked by a glycine-serine-rich flexible linker. DimAβ rapidly forms metastable off-pathway oligomers (dimAβOs) upon exceeding a COC of ~1.5 μM, which is markedly lower than that of native Aβ constructs[22,35,36]. Above this COC, dimAβ exhibits biphasic assembly kinetics, initially forming off-pathway oligomers in the first phase (Fig. 4A, phase i) that are gradually replaced by fibrils in the second phase upon prolonged incubation (Fig. 4A, phase ii). In the absence of agitation (e.g., as caused by the movement of a microplate in a fluorescence plate reader), the second phase according to fibril formation is not observed, enabling in-depth characterization of a homogenous population of metastable off-pathway oligomers free from Aβ monomers or Aβ fibrils[22]. Owing to their distinct kinetic properties compared to fibrils and their shared structural and toxic characteristics with native Aβ42 oligomers[22], dimAβOs serve as a reliable in vitro model for investigating Aβ oligomer toxicity and interactions. To study the interaction of dimAβOs with tau condensates, dimAβOs were prepared by incubation of dimAβ in the absence of any mechanical agitation, which abrogates the amyloid fibril formation phase[22]. The resulting dimAβOs, harvested after 3–4 hours of incubation, were imaged by atomic force microscopy (AFM) (Fig. 4B, image i) and DIC microscopy (Fig. S1a) prior to their application in tau interaction experiments.

To study their interaction, 4 μM dimAβO and 10 μM tau were investigated at pH 7.4 in the presence of 10% PEG. First, 10% PEG was added to tau, followed by addition of dimAβOs to the phase-separated tau and imaging using DIC microscopy. Tau in presence of dimAβOs showed similar condensates (Fig. S1b) as tau alone (Fig. 2A). The experiments were re-performed using confocal fluorescence microscopy. For this, Alexa-647-labelled tau was mixed with unlabelled tau in a molar ratio of 1:60 and Alexa-488-labelled dimAβ was mixed with unlabelled dimAβ in a molar ratio of 1:20 to generate fluorescently labelled samples. Unlike tau, fluorescently labelled dimAβOs showed no condensate formation at 10% PEG (Fig. S1c, d), and the substoichiometric addition of fluorescent labelled dimAβ did not interfere with oligomer formation (Fig. S2). In confocal microscopy a strong colocalization of both proteins was visible, hinting at recruitment of dimAβOs into tau droplets (Fig. 5A). DimAβOs explicitly exhibited a complex multiphasic re-organisation in the co-localised droplets, similar to Aβ42O-tau condensates. These multiphasic condensates showed a uniform distribution of tau. DimAβOs were dispersed throughout the entire tau droplet, but in addition showed a nested droplet-like organisation with puncta indicating clusters of high dimAβO concentration (Fig. 5B). Of note, not all tau droplets contained these puncta (Fig. S3) and the puncta exhibited variable morphologies across condensates (Fig. S4). Time-lapse imaging revealed that these nested dimAβO puncta within tau condensates persist over time without detectable changes in size or morphology, indicating comparatively rigid organization within the condensates (Fig. S5).

To test if LLPS of dimAβOs is driven by an interaction with tau or if it also occurs in the absence of tau, droplet formation in dimAβO solutions, tau solutions, and mixtures thereof was monitored by turbidity measurement. Tau displayed its characteristic turbidity increase with increasing PEG concentrations (Fig. 6A). In contrast, dimAβOs showed almost no turbidity in response to increasing PEG, indicating that the interaction with tau drives dimAβOs into the co-condensates. Addition of increasing concentrations of dimAβOs to 10 μM tau solutions did not lead to clear changes in the turbidity readout and thus did not provide evidence for a major change in condensate number or size (Fig. 6B).

To further assess changes in condensate size in the presence of dimAβOs, dynamic light scattering (DLS) measurements were performed. Particle size distributions for tau monomers, dimAβ monomers and

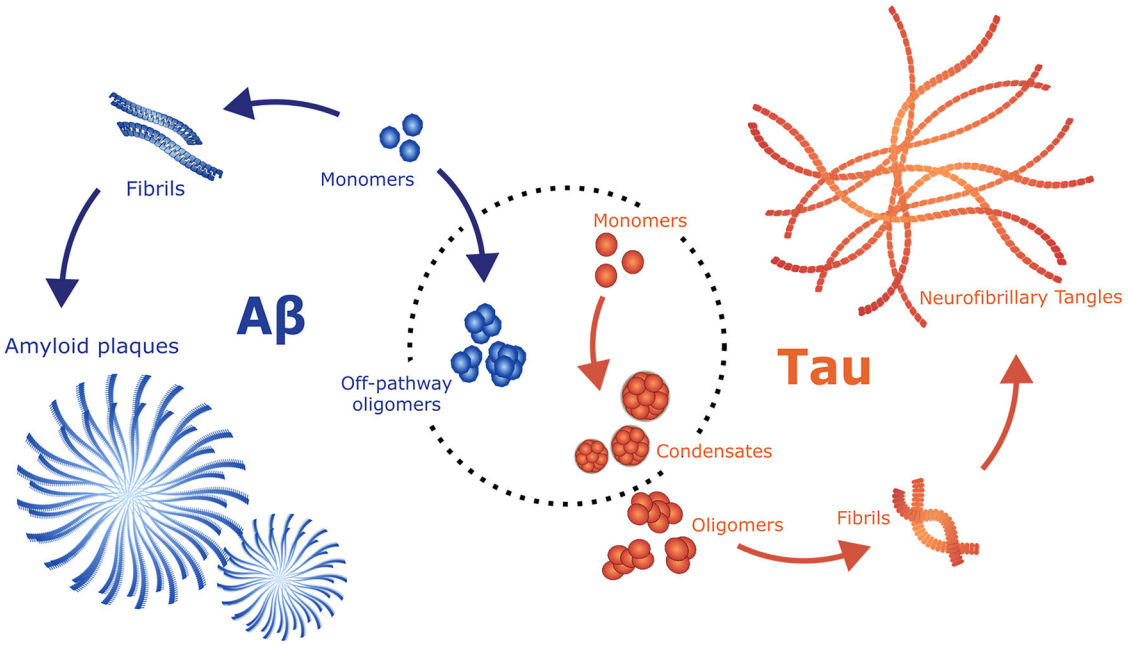

Fig. 1 | Disease-associated conformers of tau and Aβ. NFTs of tau and amyloid plaques of Aβ are the hallmark features of AD. Rather than being solely defined by tangles and plaques, AD has been studied over years as a continuum involving various toxic species of tau and Aβ. These intermediate species including oligomers and condensates play a crucial role in disease progression. Here, the interaction of tau monomers and condensates formed via LLPS with off-pathway oligomers of Aβ are explored.

dimAβOs centred around 2–10 nm, 2–5 nm and 20–100 nm, respectively (Fig. 6C, S6, 6D–F), consistent with the absence of larger aggregates[22,37]. Subsequently, the size of tau condensates in the presence and absence of dimAβOs was determined. Under LLPS conditions, tau condensates formed with a mean diameter of 2.3 µm (Fig. 6G), which increased to 3.2 µm in the presence of dimAβOs (Fig. 6H). This indicates a moderate increase in size of tau droplets upon co-condensation with dimAβOs.

DimAβOs affect dynamics of tau in the colocalized system

We used fluorescence recovery after photobleaching (FRAP) to investigate the impact of dimAβOs on tau dynamics within colocalized condensates (Fig. 7A, C, E). FRAP experiments were performed on freshly prepared Alexa-647-labelled tau with 10% PEG, using the 640 nm laser line. 25 tau droplets each in the presence/absence of dimAβOs were measured over a time period of 400 s and were subsequently analysed and compared. The results revealed a wide distribution of recovery times and immobile fractions for tau in the condensates. In the absence of dimAβOs, tau condensates showed a mean recovery half-time and immobile fraction of 46 ± 24 s and 0.25 ± 0.16, respectively, implying highly mobile, liquid-like dynamics for tau in the condensates. Upon addition of dimAβOs to the tau condensates, tau showed an increase in both the half-time of recovery and the immobile fraction in the majority of the droplets. The recovery half time of 73 ± 17 s of tau in co-condensates indicated an increase by 58% to that of tau only droplets. Similarly, the immobile fraction of the condensates increased by 68% reaching 0.42 ± 0.20 with the inclusion of dimAβOs into tau condensates. These results demonstrate that dimAβOs influence the dynamics of tau in the condensates by increasing the half-time of recovery and reducing the mobile fraction in the majority of the droplets, suggesting a decrease in the overall fluidity of the condensates. This shift toward a less dynamic state of tau indicates a pronounced effect of dimAβOs on the conformational behaviour of tau.

Broader recovery range of dimAβOs in the colocalized system

An attempt was made to explicitly study the mobility of dimAβOs in the condensates, both in the dimAβO-dense puncta and in droplets exhibiting homogeneously distributed dimAβOs. However, bleaching of the puncta was not possible due to their small size relative to the laser focus and due to their over-saturated fluorescence compared to the background. Hence, to study the dynamics of dimAβOs, condensates without puncta were selected. Similar to the earlier FRAP experiment, 25 individual recovery curves were analysed separately to determine mean half-time of recovery and the mobile dimAβO fraction in the co-droplets (Fig. 7B, D, F). This analysis yielded a mean half-time of recovery of 86 ± 60 s and an immobile fraction of 0.44 ± 0.24. Compared to tau, the recovery of dimAβOs in the co-localised droplet did not show a considerable difference, with an 18% higher recovery time and a 5% higher immobile fraction for dimAβOs (Fig. 7D, F). However, the distribution of dimAβO recovery times extended over a wider range, including high values up to 300 s. This hints at a heterogeneous population of different species and interactions of dimAβOs in the condensates.

Tau suppresses fibril formation of dimAβ by stabilizing its oligomeric form

Since dimAβOs, as AβOs in general, have neurotoxic properties[16,17,22], and we found that preformed dimAβOs interact with tau in co-condensation, we investigated a potential influence of tau on the formation of dimAβOs starting from monomeric dimAβ. As described earlier, dimAβ exhibits characteristic biphasic assembly kinetics in plate reader assays with an initial off-pathway oligomer (dimAβO) formation phase followed by a second phase in which off-pathway oligomers are gradually replaced by amyloid fibrils (Fig. 4)[22,36].

A ThT assay starting from monomeric dimAβ in the absence and presence of tau was performed both under LLPS and non-LLPS conditions. Under both conditions, the presence of tau led to a striking alteration of the characteristic biphasic aggregation kinetics of dimAβ (Fig. 8A, B, S7). While the off-pathway oligomer (dimAβO) formation phase was recovered, fibril formation was abrogated in the presence of tau. This indicates that tau does not interfere with the formation of dimAβO, and that dimAβOs are stabilized in the presence of tau inasmuch as they are not replaced by amyloid fibrils. Under non-LLPS conditions, the inhibition of the fibrillar phase was observed even at sub-stoichiometric tau concentrations (Fig. S8). To obtain structural information on these samples, AFM was performed following completion of the ThT assays. AFM imaging revealed fibrillar structures in

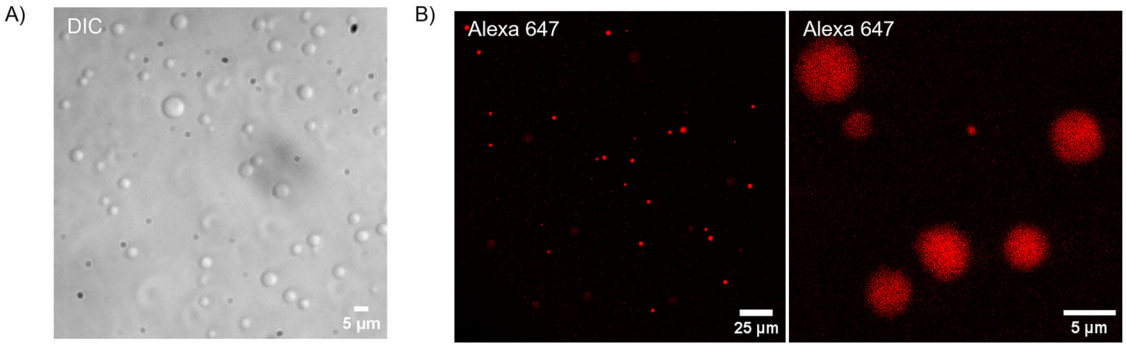

Fig. 2 | Characterization of tau LLPS. A, **B** Condensates of 10 µM tau, formed in vitro in Tris buffer (pH 7.4) with 10% PEG (PEG 6000), were imaged using (**A**) DIC microscopy and (**B**) confocal microscopy with Alexa-647-labelled tau.

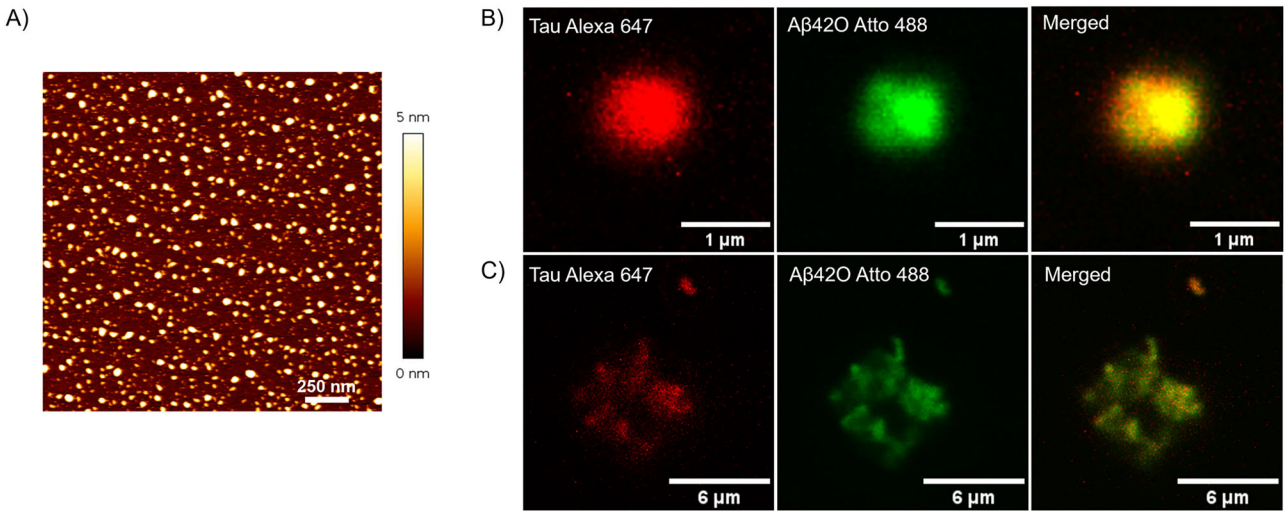

Fig. 3 | Interaction of tau with Aβ42O under LLPS conditions. A AFM image of oligomers derived from 40 µM Aβ42. Aβ42Os co-localised with 10 µM tau as (**B**) condensates and as (**C**) aggregates under LLPS conditions (See Suppl. Movies 1, 2).

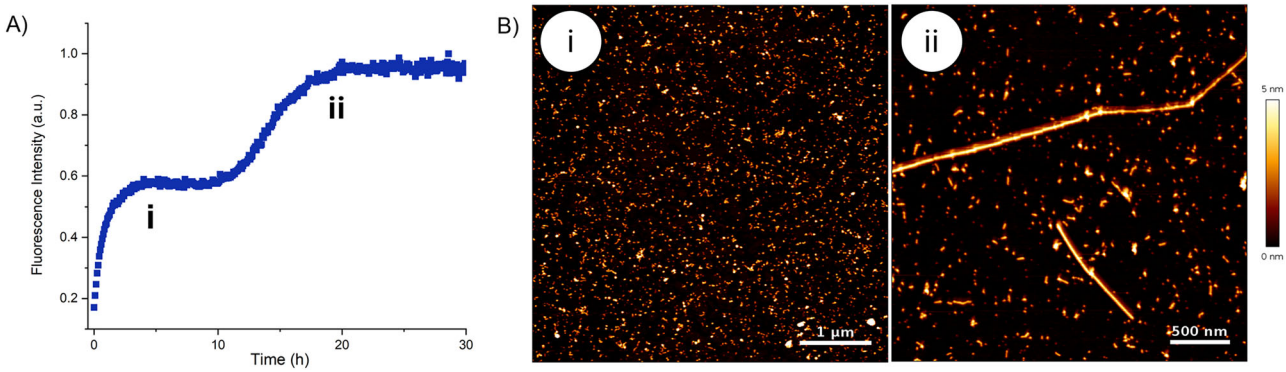

Fig. 4 | Characterization dimAβ. A ThT assay in a microplate reader depicts the biphasic kinetics of 5 µM dimAβ at pH 7.4 with an oligomer formation phase (i) followed by the replacement of oligomers with fibrils (ii). **B** AFM images corresponding to the two phases, taken after 5 h (i) and 20 h (ii). For dimAβO preparation, dimAβ incubation was not performed in a microplate reader in order to avoid any mechanical agitation. This halts dimAβ assembly at stage (i) as previously shown[22]. The source data for (**A**) is in Supplementary Data 1.

dimAβ samples without tau, both in the absence and presence of PEG (Fig. 8C i, iii). In contrast, no dimAβ fibrils were detected in samples containing tau, either in the presence or absence of crowding conditions (Fig. 8C ii, iv). Notably, amorphous, non-fibrillar accumulations were observed in samples containing tau under non-LLPS conditions. As we have found that a direct interaction of dimAβO and tau leads to their co-condensation, it is well conceivable that it is the direct interaction of dimAβO with tau that leads to kinetic stabilization of dimAβOs. These results suggest that tau stabilizes Aβ oligomers, even in the absence of crowding conditions.

Tau and dimAβOs coprecipitate in the absence of crowding agents

Arrest of dimAβ at its oligomeric phase and the presence of amorphous structures in the presence of tau indicated an intriguing interaction of tau

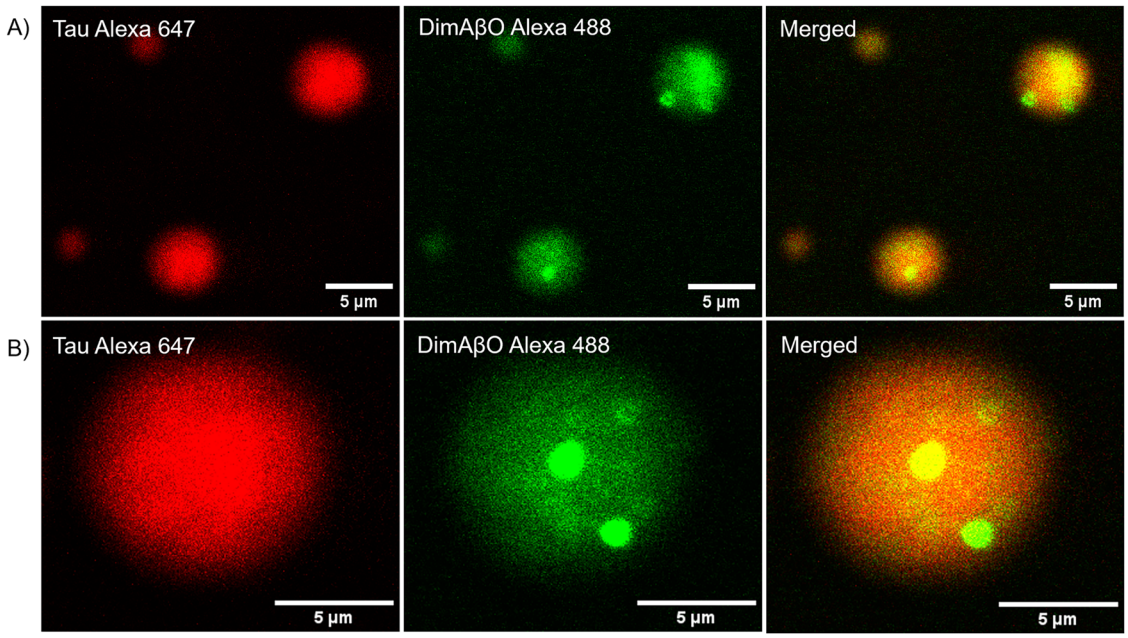

Fig. 5 | Colocalization of tau and dimAβOs. A Incubation of 10 μM of tau with 4 μM of dimAβOs in presence of 10% PEG 6000 resulted in formation of colocalized droplets within minutes of mixing. **B** Magnified view revealing detailed organisation within a tau-dimAβO droplet. DimAβOs form distinct concentrated AβO nests in the condensates. The shape and number of AβOs nests on tau condensates varied across droplets.

and dimAβOs under non-crowding conditions. Therefore, we next investigated the interaction of tau with dimAβOs in the absence of PEG. Turbidity was measured for 10 μM tau with increasing dimAβO concentrations ranging from 1 to 20 μM (Fig. 9A). Also, under non-LLPS conditions, tau-dimAβO solutions showed a high turbidity. However, in contrast to LLPS conditions (Fig. 6B), the turbidity strictly increased with increasing concentration of dimAβ (Fig. 9A). DLS experiments for 10 μM tau and 10 μM dimAβ showed the existence of particles in the size range up to 50 μm with a mean diameter of 7–8 μm (Fig. 9B). Imaging of the coprecipitates by DIC revealed amorphous aggregates, indicating that dimAβOs form large clusters upon interaction with tau under non-LLPS conditions (Fig. 9C). Imaging using AFM substantiated the results from DIC microscopy and showed the presence of amorphous aggregates (Fig. 9C) and absence of any fibrillar structures as observed in Fig. 8D (iv). Fluorescence microscopy with labelled Alexa647-tau and Alexa488-dimAβ, mixed in the same ratio as used for the LLPS experiments, confirmed the colocalization of tau and dimAβO in these aggregates (Fig. 9D). Subsequent FRAP experiments showed little to no fluorescence recovery in both tau and dimAβOs, implying a solid and immobile nature of the aggregates (Fig. S9).

To assess the cytotoxicity of tau-dimAβO co-aggregates, lactate dehydrogenase (LDH) release assays were performed using SH-SY5Y cells. Cells at the desired confluency were exposed to tau alone, dimAβOs alone, or preformed tau-dimAβO co-aggregates and monitored for 72 hours. LDH measurements at 72 h showed that treatment with dimAβOs resulted in increased LDH release compared to control, whereas tau alone and tau-dimAβO co-aggregates were associated with lower levels of cytotoxicity (Fig. S10). These data suggest that co-aggregation with tau is associated with reduced acute cytotoxicity of dimAβO.

Intracellular behaviour of tau-dimAβO co-assemblies

To study the stability and potential formation of tau and dimAβO co-assemblies in a cellular context, preformed co-condensates and co-aggregates were introduced into HEK293T cells by transfection. For transfection, fluorescently labelled tau and dimAβOs were used, and the co-assemblies were prepared like for the in vitro experiments described above, i.e., by coincubation of 4 μM dimAβOs and 10 μM tau at pH 7.4 in the presence or absence of 10% PEG. Transfection was performed using a standard protocol, after which nuclei were stained with DAPI, and cells were imaged in the corresponding fluorescence channels for tau and dimAβOs. Fluorescence imaging revealed that, following transfection, tau-dimAβO co-condensates were readily observed within cells, where they remained stable and co-localized in the intracellular environment (Fig. 10A). In contrast, tau-dimAβO co-aggregates were infrequently detected within cells and were predominantly observed as extracellular deposits (Fig. 10B).

Discussion

Two key proteins central to AD pathology are tau and Aβ, and their pathological deposits are hallmark features of the disease. Both proteins have been extensively studied and increasing evidence suggests they contribute synergistically to the disease progression[28,38]. A bidirectional interplay between tau and Aβ has been demonstrated in AD pathology. Aβ directly affects tau pathology by accelerating tau phosphorylation, inducing tau oligomer formation, and promoting tau aggregation by cross-seeding and spreading[28,38,39]. Conversely, tau enhances Aβ toxicity and together they damage mitochondria, ultimately leading to neuronal death under pathological conditions[40]. In the context of these synergistic activities, the question has been posed if they arise from a direct interaction between tau and Aβ[38]. Here, we find that tau readily interacts with off-pathway oligomers of Aβ leading to changes in the assembly dynamics of both proteins.

Strikingly, presence of tau arrests dimAβ assembly at the off-pathway oligomeric stage. Tau effectively sequesters AβOs either in amorphous co-aggregates under non-LLPS conditions, or in tau droplets under LLPS conditions. While the LDH release assay data suggests that this sequestration reduces acute Aβ oligomer toxicity, it may on the other hand extend long-term exposure to Aβ oligomers by prolonging their bioactive state. Consistent with our findings, previous studies have shown that tau interfered with fibril formation of Aβ by disrupting elongation and secondary aggregation processes[33,41]. Similarly, Aβ fibril formation was inhibited upon its sequestration within biomolecular condensates formed by multi-domain proteins containing low complexity domains (LCDs)[42].

Recently, tau was studied to undergo phase separation, forming protein-dense condensates that can potentially initiate pathogenic tau fibril formation[9]. Our results show that tau droplets could also be the sites of direct tau-Aβ interaction. AβOs slow down the dynamics of tau in the co-localized

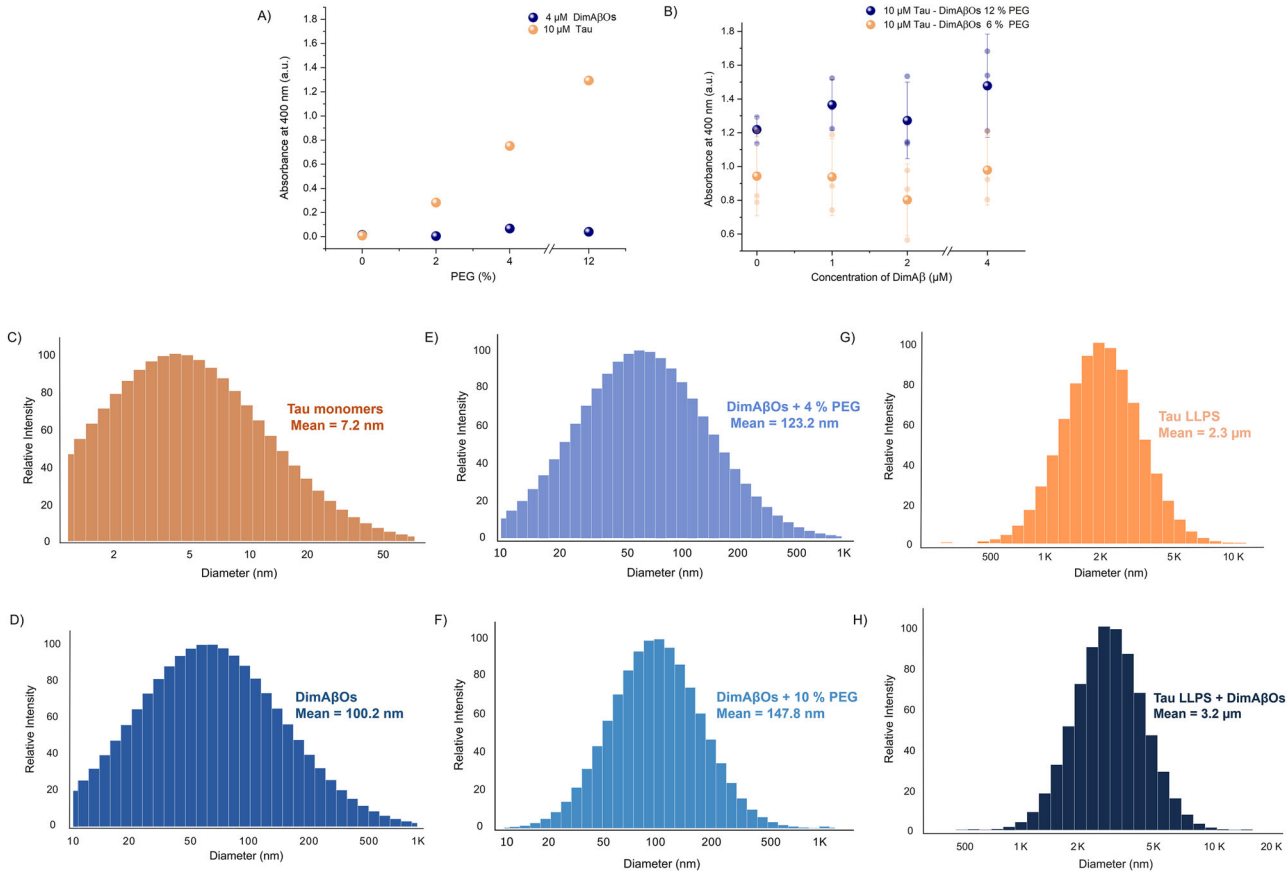

Fig. 6 | Turbidity and DLS measurements. A, B Absorbance measurements at 400 nm indicating turbidity of (**A**) either tau or dimAβOs titrated with increasing concentrations of PEG, (**B**) tau titrated with increasing concentrations of dimAβOs and PEG (displayed is the mean of $n = 3$ biologically independent samples, error bars represent SD). **C-H)** Particle size distribution determined by DLS of (**C**) 10 µM tau monomers, (**D**) 4 µM dimAβOs, (**E, F**) 4 µM dimAβOs with different concentrations of crowding agent, (**G**) tau condensates at a concentration of 10 µM tau and (**H**) tau-dimAβO co-condensates at concentrations of 10 µM tau and 4 µM dimAβOs. The source data for (**A**, **B**) is in Suppl. Data 1.

droplets and reduce the overall mobile fraction of tau in the condensates. This could originate from a dense network of tau and AβO interactions, or from a faster maturation of tau inside the co-condensates as observed in the case of tau mutations[43]. Outside of the dimAβO puncta, the half-time of recovery in FRAP for dimAβOs was similar to that of tau. For technical reasons we could not determine the dynamics of dimAβOs within the puncta, and therefore we cannot evaluate potential differences in AβO dynamics within these nested droplets.

The nested droplets represent an interesting "phase within phase" organisation within the tau-AβO coacervates. This hierarchical structuring has been previously observed in several functional systems including nucleoli[44,45], stress granules[46], and anisosomes[47]. This type of layering helps in efficient biochemical compartmentalization and functioning within membraneless organelles. Tau has previously been shown to form multiphasic condensates with prion protein (PrP), exhibiting unique multiphasic layering influenced by the RNA concentration[48]. Previous studies have suggested that differences in physicochemical properties, including micropolarity and interfacial characteristics, can influence the formation of multiphasic organization in condensates[49,50]. In systems where components differ in these properties, spatial segregation within condensates has been observed[51,52]. In the present study, we note that AβOs preferentially localize into nested subdomains within tau-rich condensates. While we do not directly measure interfacial tension or polarity in this system, such physicochemical differences may contribute to the observed internal organization.

The stability of tau-AβO condensates in a cellular environment adds to the physiological relevance of this interactive system. Earlier studies show that overexpressing tau can form condensates in cells, raising the possibility that tau-AβO condensates may form under pathological or stress-related conditions[10]. Biomolecular condensates have been proposed to function both as hotspots that accelerate amyloid formation and as 'safe reservoirs' that sequester amyloidogenic proteins[42,53]. Hence, characterizing the functional nature of these co-condensates in a cellular environment will be important for interpreting their pathological relevance.

In contrast to condensate formation, tau-AβO aggregates were predominantly observed as extracellular deposits. This observation highlights the distinct behaviours of tau-Aβ assemblies and suggests that co-condensates and co-aggregates may affect cellular function through divergent mechanisms. Cellular toxicity measured by LDH release reveal that tau reduces the toxicity of AβOs upon co-aggregation. This observation is consistent with previous studies showing that non-phosphorylated tau monomers can bind to Aβ42Os and reduce its toxicity[41].

Regarding the limitations of this study, it should be noted that further studies in complementary cellular systems will be required to provide evidence for the physiological relevance of these co-aggregates for neuronal health. For example, optogenetic systems in which tau clustering is controlled with light are promising tools that can give insight into tau condensation and aggregation in cells[54–56]. Furthermore, while our study establishes interaction and co-condensation of AβOs with tau, the molecular determinants of this interaction remain unresolved and will require future domain-specific structural investigations. As discussed above, FRAP was only possible for tau droplets with homogeneously distributed dimAβO, not for the nested dimAβO droplets. The dynamics and structural organization of the nested droplets thus require further investigation.

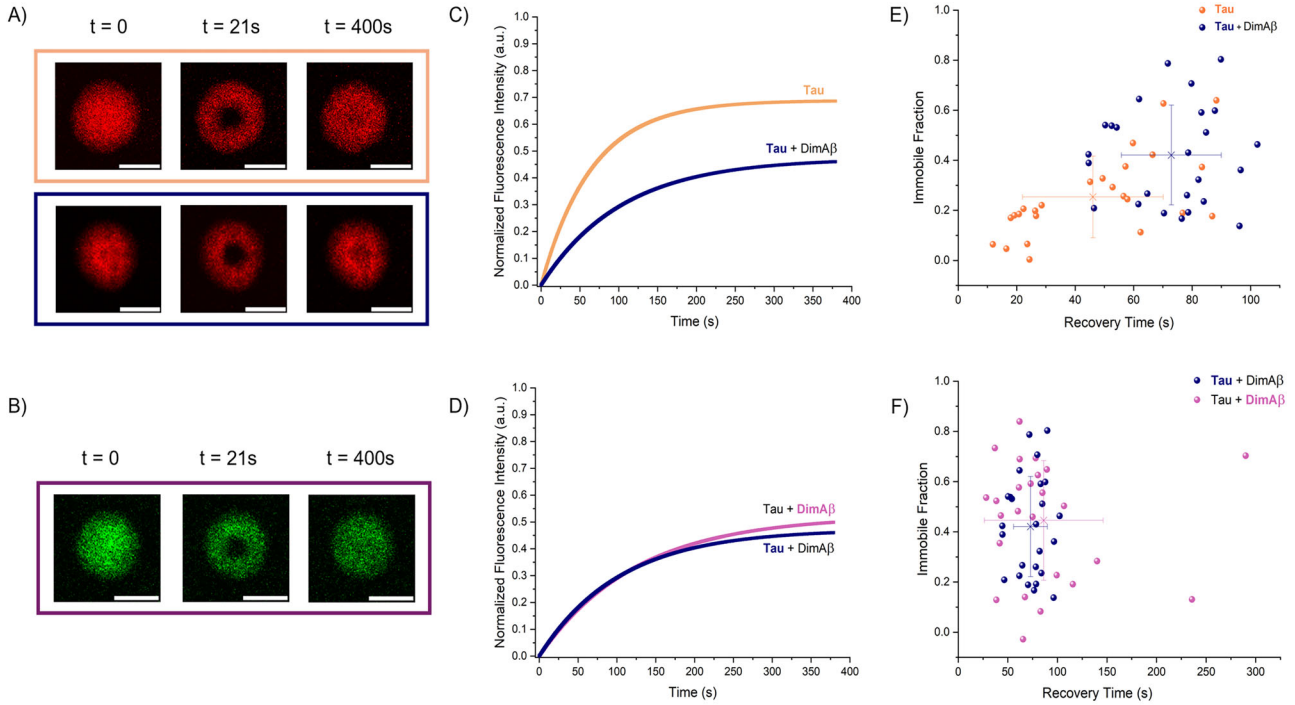

Fig. 7 | Dynamics of tau and dimAβOs in the condensates. A, **B** Time series of images captured during FRAP experiments using a 640 nm and a 488 nm laser line, visualising tau (**A**) and dimAβOs (**B**), respectively. The experiments were performed at 10 μM tau and 4 μM dimAβOs in the presence of 10% PEG. To determine the dynamics of tau in the condensates, individual analysis of 25 independent experiments ($n = 25$) was conducted. In each case, a region of interest (ROI), mostly central to the droplets was photobleached, and fluorescence recovery was analysed to assess protein mobility. Scale bar: 5 μm. **C** Recovery curves of tau in the condensates +/− dimAβOs, depicting the mean values for half time of recovery and mobile fraction of tau in the respective cases. **D** Recovery curves depicting the mean of recovery of dimAβOs compared with the recovery of tau in the co-condensates. **E**, **F** Individual half-recovery times and immobile fractions from each of the independent experiments ($n = 25$ independent experiments); mean ± SD indicated by crosshairs. The source data for (**C**–**F**) is in Suppl. Data 1.

The ability of tau to capture other proteins into its condensates is now increasingly studied. Post-translational modifications and presence of flexible disordered regions in tau enables it to adopt multiple conformations that can interact with a variety of binding partners[57]. Tau undergoes heterotypic phase separation with alpha-synuclein[58], TIA1[59], and PrP[60], suggesting a synergistic interplay that may contribute to the progression of diseases[61]. Intriguingly, it has been shown that the cellular prion protein (PrP) interacts with both Aβ and tau at the neuronal membrane and mediates Aβ-induced tau pathology[62]. Our findings that tau undergoes heterotypic condensation with AβOs, together with prior evidence of condensation of tau with PrP[48], suggest that phase separation may be a central mechanism underlying these pathogenic interactions.

Methods

Protein expression and purification

pET-28a vector containing the gene for full-length 4R-Tau (hTau40) was transformed into *Escherichia coli* BL21(DE3) cells. Cells were grown in 2YT with kanamycin (50 μg/mL) at 37 °C and induced at OD 0.6 with 1 mM of isopropyl D-thiogalactopyranoside (IPTG). Cells were further grown for 4 h and subsequently harvested. Cells were lysed with 20 mM PIPES buffer, 500 mM NaCl, 2 mM dithiothreitol (DTT), pH 6.5, complemented by a protease inhibitor tablet (Roche Applied Sciences). The lysed cells were sonicated for 5 min at 3 sec pulse, 5 seconds pause, which was repeated for a total of three times. The cell debris was then removed by centrifugation at 40,000 g, 4 °C, for 40 min. The supernatant was then heated at 80 °C for 15 min owing to the thermal stability of tau and the centrifugation was repeated to remove all denatured proteins. 54% ammonium sulphate was used to precipitate tau from the clear supernatant overnight and the pellet with tau was collected by centrifugation the next day. The pellet was resuspended in ddH_2O and dialysed to 20 mM PIPES buffer, 50 mM NaCl, 2 mM DTT, pH 6.5. After overnight dialysis to the desired buffer, purification of tau was continued using ion exchange chromatography (IEC) with HiTrap SP FF (5 mL) column and eluted with a linear gradient of 1 M NaCl, PIPES buffer, 2 mM DTT, pH 6.5. Size exclusion chromatography was then performed on a Hi-Load 16/600 Superdex 75 pg column to remove truncation products and protein was re-buffered into 30 mM Tris, 50 mM NaCl, pH 7.4, as the final step. Purification of dimAβ was performed as described in ref. 22.

Protein fluorescent labelling

Tau was labelled with Alexa-647 NHS ester (Thermo Fisher Scientific, catalog number A20006). For labelling, 3 mg of lyophilized tau dissolved in 90 mM HEPES/NaOH, pH 7.9, 10% amine-free DMF, was incubated with excess dye for ca. 70–90 min at 20 °C in the dark. Excess dye was subsequently removed by HPLC on a Zorbax SB300 C8 9.4 × 250 mm semi-preparative column. To obtain fluorescently labelled dimAβ, a variant with a cysteine at position 0 was conjugated with Alexa488-maleimide by suspension in a small volume of 50 mM NaOH followed by dilution into 1 mM DTT, 300 mM HEPES, pH 7, and addition of the same small volume of 50 mM HCl. Thereafter, the Alexa488-maleimide was added and left to react for 30 min before purification by HPLC. For confocal microscopy labelled and unlabelled protein were mixed in the ratio of 1:60 for tau and 1:20 for dimAβ and were briefly incubated at room temperature before aliquoting. For preparing fluorescently labelled Aβ42, Atto488-Cys0Aβ42 was mixed with unlabelled Aβ42 in the ratio of 1:20 and briefly incubated at room temperature before use in experiments.

Preparation of Aβ42 oligomers

Oligomers from native Aβ42 construct were prepared to study their interaction with tau. 1 mg aliquot of Aβ42 from BACHEM (CAS Number: 107761-42-2) was first dissolved in HFIP, aliquoted and lyophilised. After lyophilisation, each aliquot was first dissolved in 50 μL 50 mM NaOH and

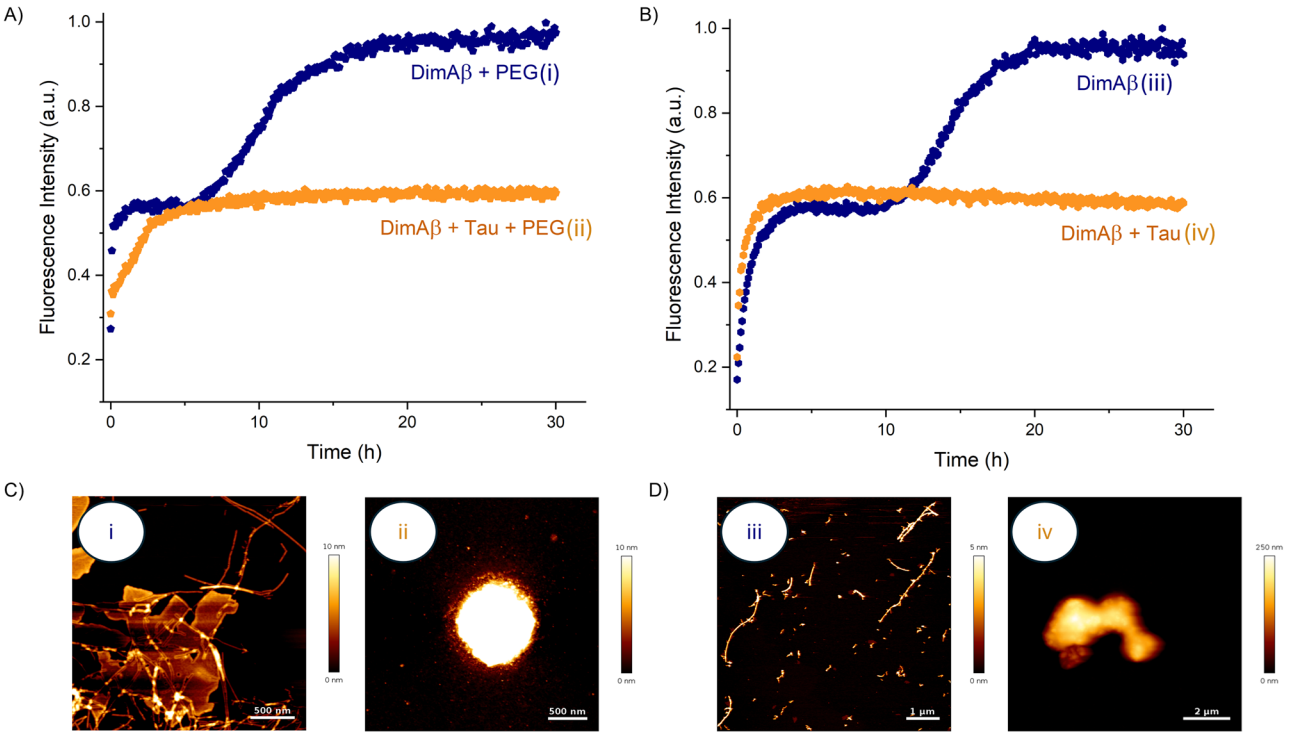

Fig. 8 | Effect of tau and PEG on the aggregation kinetics of dimAβ. A, **B** Assembly kinetics of 5 µM dimAβ at 37 °C and pH 7.4 in the presence (orange) or absence (blue) of 10 µM tau under (**A**) LLPS conditions or (**B**) non-LLPS conditions. The corresponding data for two further dimAβ concentrations is shown in Fig. S7. **C**, **D** AFM images corresponding to the ThT assays under (**C**) LLPS and (**D**) non-LLPS conditions. The source data for (**A**, **B**) is in Supplementary Data 1.

sonicated for 30 s in water bath. After dissolution, it was further added with 20 mM NaPi at pH 7.4, followed by 50 µL of HCl. For preparation of oligomers, 40 µM Aβ42 was incubated at 37 °C for 2 h and was used for experiments.

Preparation of dimAβ oligomers

DimAβ was initially resuspended in a small volume of 50 mM NaOH, followed by the addition of the appropriate buffer. The pH was then adjusted by titration with an equal volume of 50 mM HCl. The stock solution prepared at higher concentrations (50–60 µM), was subsequently diluted to the desired concentration and incubated at 37 °C for 3–4 h. Oligomerization was confirmed by AFM imaging before experiments.

LLPS tau

Unless mentioned specifically, all tau condensates were prepared at a concentration of 10 µM in 30 mM Tris, 50 mM NaCl, pH 7.4, with 10% PEG 6000 (SigmaAldrich-81260). To image the droplets, 5–6 µL of the solution were placed on a clean glass slide with a coverslip on top to prevent evaporation.

ThT aggregation kinetics

For the dimAβ ThT assays, ThT, NaN_3, NaCl, and protein were prepared in a mixture of MOPS and Tris buffer at pH 7.4 such that the desired protein concentration and concentrations of 20 µM ThT, 0.05% NaN_3, and 150 mM NaCl were reached in a total volume of 100 µL. The measurement was performed in a 96-well low-binding plate (Greiner) in a BMG FluoStar Omega reader. Data points were collected at 37 °C every 5 min using the BMG Reader Control software (version 5.40).

Turbidity measurement and DLS

Turbidity of the protein mixtures was recorded from the optical density at 400 nm, measured with a Jasco V-650 spectrophotometer. All the samples were prepared shortly before their measurement. DLS was performed on a submicron particle sizer, Nicomp 380 (Particle Sizing Systems Nicomp). Data was analysed with the Nicomp algorithm using the intensity-weighted Gaussian distribution analysis. The sample was measured for 3 cycles, and the average distribution was generated. For samples containing 10% PEG 6000, a refractive index of 1.34 and viscosity of 2.5 cp was taken into account.

Fluorescence recovery after photobleaching (FRAP)

FRAP experiments were done on in vitro droplets formed by Alexa647-tau: tau (1:60) with Alexa488-Cys0-dimAβ: dimAβ (1:20) using 640 nm and 488 nm laser lines, respectively, imaged on a Olympus FV3000 microscope with a 60x UPLSAPO water immersion objective. To minimize photobleaching during acquisition, low laser transmission settings were used. For every droplet of interest (diameter approx. 3 µm) pre-bleach frames (1 s frame rate, 20 frames) were recorded, followed by bleaching a spot on the droplet (tornado ROI;1 s) at 100% transmission in the respective laser lines, and post-bleach images were collected (1 s frame rate, 380 frames). For every experiment, all the parameters were conserved, and the mean fluorescence intensities of three regions, namely ROI1 = photobleached region inside a droplet, ROI2 = the whole droplet of interest, and ROI3 = background signal outside the droplet, were recorded. The recovery curves were corrected for background and fluorescence loss and normalized with easyFRAP[63], and the resulting data was analysed in OriginPro 2021b following the exponential growth model $A\left(1 - e^{-kx}\right)$.

Differential interference contrast microscopy (DIC)

DIC imaging of condensates and aggregates was performed using a Leica Infinity TIRF microscope operated in DIC mode via Leica LAS AF software. For imaging, 6 µL of each sample was placed onto a 60 × 24 mm glass coverslip and overlaid with a 20 × 20 mm coverslip. Images were acquired using a Leica HCX PL APO 100×/1.47 NA oil immersion objective. Image analysis and processing were carried out using FIJI software (ImageJ, version 1.54 f).

Atomic force microscopy (AFM)

For observing Aβ42 and dimAβ oligomers and fibrils and amorphous aggregates of tau and dimAβ, 3 µL of each respective sample were applied

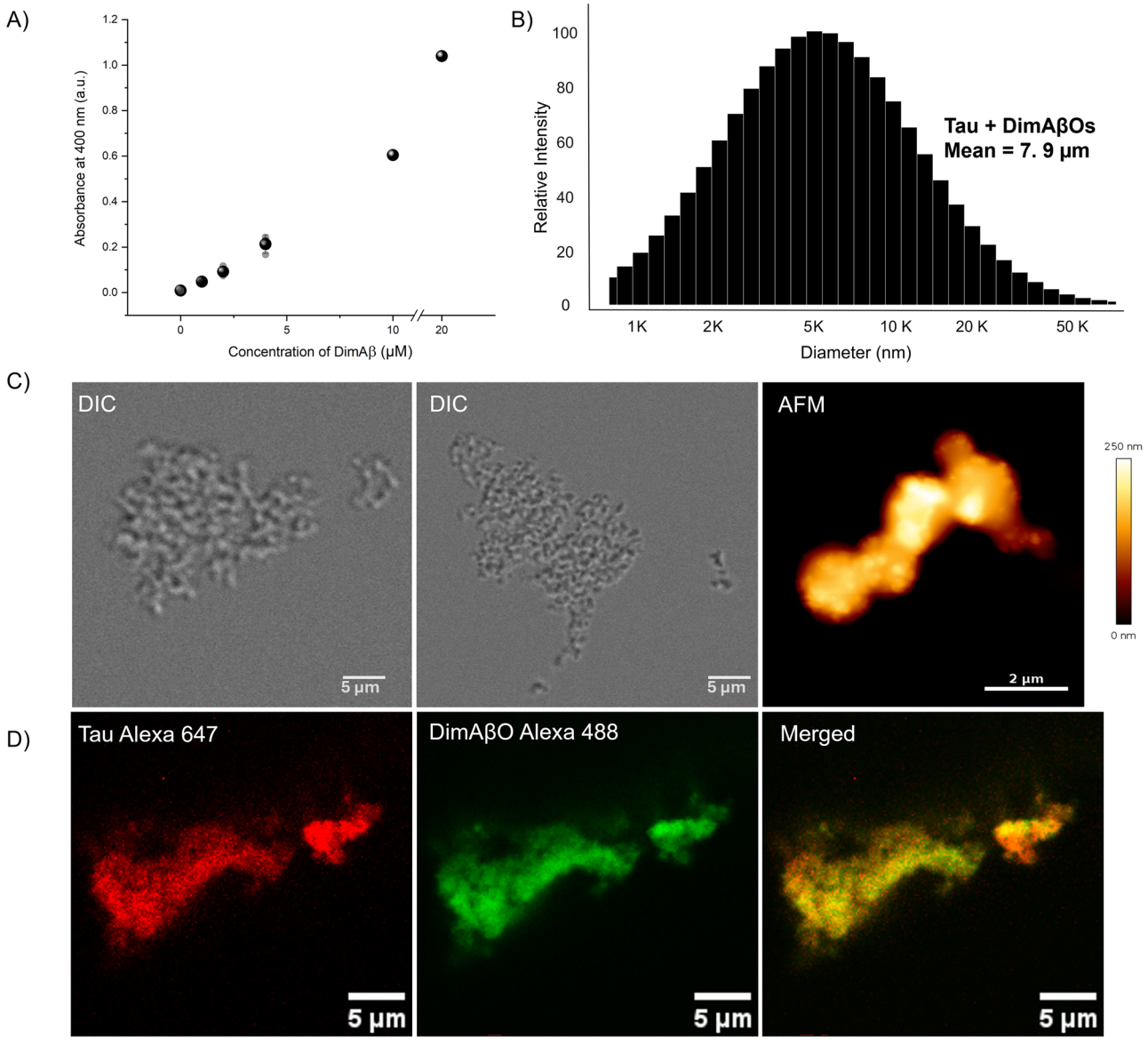

Fig. 9 | Interaction of tau and dimAβOs under non-LLPS conditions. A Turbidity measurements of 10 μM tau with dimAβOs (1–20 μM) show a concentration-dependent increase in turbidity (displayed is the mean of $n = 3$ biologically independent samples, error bars represent SD). **B** DLS analysis revealed presence of particles up to ~50 μm in diameter. **C** DIC microscopy showed the presence of large, heterogeneous clusters and were further supported by AFM imaging. **D** Fluorescence microscopy of labelled proteins indicated co-aggregate formation. The source data for (**A**) is in Suppl. Data 1.

onto freshly cleaved muscovite mica. The samples were left to dry, washed with 500 μL ddH_2O, and dried with a stream of N_2 gas. Imaging was performed in intermittent contact mode (AC mode) in a JPK Nano Wizard 3 atomic force microscope (JPK) using a silicon cantilever with silicon tip (either Olympus OMCL-AC160TS-R3 with a typical tip radius of 9 ± 2 nm, a force constant of 26 N/m and resonance frequency around 250 kHz, or Olympus OMCL-AC240TS with a typical tip radius of 9 ± 2 nm, a force constant of 0.5–4.4 N/m and a resonance frequency around 65 kHz). The choice of tip was made solely for reasons of availability. The images were processed using JPK DP Data Processing Software (version spm-5.0.84). For the presented images, a polynomial fit was subtracted from each scan line first independently and then using a limited data range.

Transfection assays

HEK293T cells (ATCC) were maintained in high-glucose Dulbecco's modified Eagle's medium (DMEM; Sigma-Aldrich) supplemented with 10% (v/v) foetal calf serum (Sigma-Aldrich), 50 U/mL penicillin, and 50 μg/mL streptomycin (Sigma-Aldrich) at 37 °C in a humidified atmosphere containing 5% CO_2. For transfection assays, cells were seeded into poly-D-lysine–coated 384-well plates (Greiner) at a density of 7000 cells per well in 70 μL of culture medium supplemented with 0.1 μg/mL Hoechst 33342 (Thermo Fisher Scientific). Co-droplets and co-aggregates were prepared as described previously and incubated with 1.5% (v/v) Lipofectamine in Opti-MEM for 2 h at room temperature. Subsequently, 10 μL of the transfection mixture was added to each well 4 h after cell seeding. Plates were incubated for an additional 2 h at 37 °C and 5% CO_2 prior to imaging using an IN Cell Analyzer 6500HS system (Cytiva). Image processing and figure preparation were performed using ImageJ2 (v2.16.0/1.54p), GIMP (v3.0.6), and Inkscape (v1.3.2).

Cell toxicity assay-LDH

Human neuroblastoma SH-SY5Y cells (DSMZ) were maintained in Dulbecco's Modified Eagle Medium/Nutrient Mixture F-12 (DMEM/F-12) supplemented with 10% fetal bovine serum, 1% non-essential amino acids, and 1% penicillin–streptomycin at 37 °C in a humidified incubator with 5% CO_2. Cells were seeded in 96-well plates at a density of 4200 cells per well in a

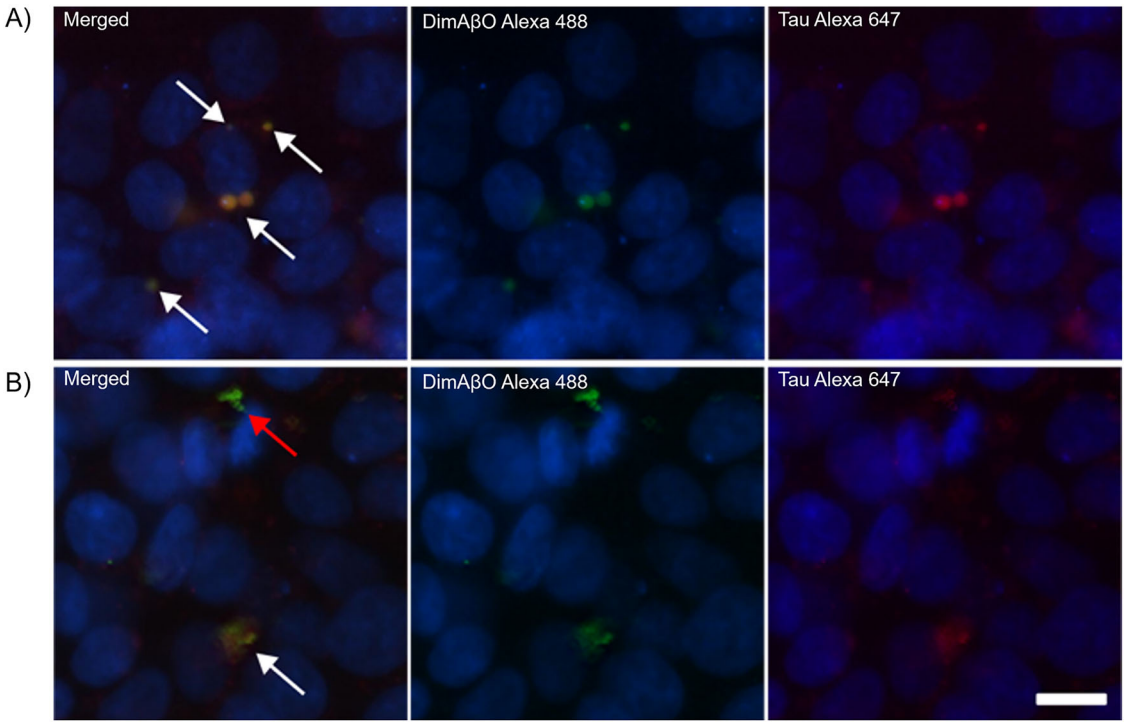

Fig. 10 | Differential intracellular behaviour of tau-dimAβO co-assemblies following transfection. A Tau-dimAβO co-condensates (white arrows) localize intracellularly following transfection into HEK293T cells (left, center, and right panels). **B** Tau-dimAβO co-aggregates formed under non-LLPS conditions are predominantly extracellular (red arrow), with rare intracellular presence (white arrow). Nuclei are stained with DAPI (blue). Scale bar: 10 μm (right panel in **B**), applies to all panels.

total volume of 100 μL and allowed to adhere for 24 h. LDH release was quantified using the CyQUANT™ LDH Cytotoxicity Assay Kit (Thermo Fisher Scientific) according to the manufacturer's instructions. Briefly, 50 μL of culture supernatant from each well was transferred to a new 96-well plate and mixed with 50 μL of reaction mixture prepared by combining assay buffer with substrate solution. Following incubation for 30 min at room temperature protected from light, 50 μL of stop solution was added. The absorbance of each condition was measured at 490 nm and 680 nm using multi-detection plate reader (Tecan Safire 2). LDH release was calculated by subtracting background absorbance (680 nm) from the primary signal (490 nm) and normalizing values to the baseline control to obtain fold change. Statistical analysis was performed using one-way ANOVA followed by Bonferroni's post hoc test in OriginPro 2021b. Data are presented as mean ± SEM from independent experiments.

Data availability

The source data underlying Figs. 4A, 6A, 6B, 7C, 7D, 7E, 7F, 8A, 8B and 9A are provided in Supplementary Data 1. Other relevant data are available from the corresponding author upon request.

Received: 13 April 2026; Accepted: 30 July 2026;
Published online: 10 August 2026

References

1. Kovacs, G. G. Tauopathies. *Handb. Clin. Neurol.* **145**, 355–368 (2017).
2. Gendron, T. F. & Petrucelli, L. The role of tau in neurodegeneration. *Mol. Neurodegener.* **4**, 13 (2009).
3. Kadavath, H. et al. Tau stabilizes microtubules by binding at the interface between tubulin heterodimers. *Proc. Natl. Acad. Sci.* **112**, 7501–7506 (2015).
4. Barbier, P. et al. Role of Tau as a microtubule-associated protein: structural and functional aspects. *Front. Aging Neurosci.* **11**, 204 (2019).
5. Nizynski, B., Dzwolak, W. & Nieznanski, K. Amyloidogenesis of Tau protein. *Protein Sci* **26**, 2126–2150 (2017).
6. Scheres, S. H., Zhang, W., Falcon, B. & Goedert, M. Cryo-EM structures of tau filaments. *Curr. Opin. Struct. Biol.* **64**, 17–25 (2020).
7. Wang, B. et al. Liquid–liquid phase separation in human health and diseases. *Signal Transduct. Target. Ther.* **6**, 1–16 (2021).
8. Alberti, S., Gladfelter, A. & Mittag, T. Considerations and challenges in studying liquid-liquid phase separation and biomolecular condensates. *Cell* **176**, 419–434 (2019).
9. Ambadipudi, S., Biernat, J., Riedel, D., Mandelkow, E. & Zweckstetter, M. Liquid–liquid phase separation of the microtubule-binding repeats of the Alzheimer-related protein Tau. *Nat. Commun.* **8**, 275 (2017).
10. Wegmann, S. et al. Tau protein liquid–liquid phase separation can initiate tau aggregation. *EMBO J* **37**, e98049 (2018).
11. Hernández-Vega, A. et al. Local nucleation of microtubule bundles through tubulin concentration into a condensed Tau Phase. *Cell Rep*. **20**, 2304–2312 (2017).
12. Vanderweyde, T. et al. Interaction of tau with the RNA-Binding Protein TIA1 Regulates tau Pathophysiology and Toxicity. *Cell Rep*. **15**, 1455–1466 (2016).
13. Ferreon, J. C. et al. Acetylation disfavors Tau phase separation. *Int. J. Mol. Sci.* **19**, 1360 (2018).
14. Goedert, M. et al. Assembly of microtubule-associated protein tau into Alzheimer-like filaments induced by sulphated glycosaminoglycans. *Nature* **383**, 550–553 (1996).
15. Chen, G. et al. Amyloid beta: structure, biology and structure-based therapeutic development. *Acta Pharmacol. Sin.* **38**, 1205–1235 (2017).
16. Hayden, E. Y. & Teplow, D. B. Amyloid β-protein oligomers and Alzheimer's disease. *Alzheimers Res. Ther.* **5**, 60 (2013).
17. Viola, K. L. & Klein, W. L. Amyloid β oligomers in Alzheimer's disease pathogenesis, treatment, and diagnosis. *Acta Neuropathol. (Berl.)* **129**, 183–206 (2015).

18. Alberdi, E. et al. Amyloid beta oligomers induce Ca^{2+} dysregulation and neuronal death through activation of ionotropic glutamate receptors. *Cell Calcium* **47**, 264–272 (2010).
19. Resende, R., Ferreiro, E., Pereira, C. & Resende de Oliveira, C. Neurotoxic effect of oligomeric and fibrillar species of amyloid-beta peptide 1-42: involvement of endoplasmic reticulum calcium release in oligomer-induced cell death. *Neuroscience* **155**, 725–737 (2008).
20. Muschol, M. & Hoyer, W. Amyloid oligomers as on-pathway precursors or off-pathway competitors of fibrils. *Front. Mol. Biosci.* **10**, 1120416 (2023).
21. Dear, A. J. et al. Identification of on- and off-pathway oligomers in amyloid fibril formation. *Chem. Sci.* **11**, 6236–6247 (2020).
22. Schützmann, M. P. et al. Endo-lysosomal Aβ concentration and pH trigger formation of Aβ oligomers that potently induce Tau missorting. *Nat. Commun.* **12**, 4634 (2021).
23. Soto, C. & Pritzkow, S. Protein misfolding, aggregation, and conformational strains in neurodegenerative diseases. *Nat. Neurosci.* **21**, 1332–1340 (2018).
24. Hernandez, P., Lee, G., Sjoberg, M. & Maccioni, R. B. Tau phosphorylation by cdk5 and Fyn in response to amyloid peptide Abeta (25-35): involvement of lipid rafts. *J. Alzheimers Dis*. *JAD* **16**, 149–156 (2009).
25. Nygaard, H. B. Targeting Fyn Kinase in Alzheimer's Disease. *Biol. Psychiatry* **83**, 369–376 (2018).
26. Ittner, L. M. et al. Dendritic function of tau mediates amyloid-beta toxicity in Alzheimer's disease mouse models. *Cell* **142**, 387–397 (2010).
27. Sperling, R. A. et al. The impact of amyloid-beta and tau on prospective cognitive decline in older individuals. *Ann. Neurol.* **85**, 181–193 (2019).
28. Bloom, G. S. Amyloid-β and tau: the trigger and bullet in Alzheimer disease pathogenesis. *JAMA Neurol* **71**, 505–508 (2014).
29. Vergara, C. et al. Amyloid-β pathology enhances pathological fibrillary tau seeding induced by Alzheimer PHF in vivo. *Acta Neuropathol. (Berl.)* **137**, 397–412 (2019).
30. Vasconcelos, B. et al. Heterotypic seeding of Tau fibrillization by pre-aggregated Abeta provides potent seeds for prion-like seeding and propagation of Tau-pathology in vivo. *Acta Neuropathol. (Berl.)* **131**, 549–569 (2016).
31. Manczak, M. & Reddy, P. H. Abnormal interaction of oligomeric amyloid-β with phosphorylated tau: implications to synaptic dysfunction and neuronal damage. *J. Alzheimers Dis*. *JAD* **36**, 285–295 (2013).
32. He, Z. et al. Amyloid-β plaques enhance Alzheimer's brain tau-seeded pathologies by facilitating neuritic plaque tau aggregation. *Nat. Med.* **24**, 29–38 (2018).
33. Wallin, C. et al. The Neuronal Tau Protein Blocks in Vitro Fibrillation of the Amyloid-β (Aβ) Peptide at the Oligomeric Stage. *J. Am. Chem. Soc.* **140**, 8138–8146 (2018).
34. Miti, T., Mulaj, M., Schmit, J. D. & Muschol, M. Stable, Metastable, and Kinetically Trapped Amyloid Aggregate Phases. *Biomacromolecules* **16**, 326–335 (2015).
35. Hasecke, F. et al. Origin of metastable oligomers and their effects on amyloid fibril self-assembly. *Chem. Sci.* **9**, 5937–5948 (2018).
36. Hasecke, F. et al. Protofibril-fibril interactions inhibit amyloid fibril assembly by obstructing secondary nucleation. *Angew. Chem. Int. Ed Engl.* **60**, 3016–3021 (2021).
37. Prince, P. R. et al. Initiation and modulation of Tau protein phase separation by the drug suramin. *Sci. Rep.* **13**, 3963 (2023).
38. Busche, M. A. & Hyman, B. T. Synergy between amyloid-β and tau in Alzheimer's disease. *Nat. Neurosci.* **23**, 1183–1193 (2020).
39. Roda, A. R., Serra-Mir, G., Montoliu-Gaya, L., Tiessler, L. & Villegas, S. Amyloid-beta peptide and tau protein crosstalk in Alzheimer's disease. *Neural Regen. Res.* **17**, 1666–1674 (2022).
40. Zhang, H. et al. Interaction between Aβ and Tau in the Pathogenesis of Alzheimer's Disease. *Int. J. Biol. Sci.* **17**, 2181–2192 (2021).
41. Beeg, M. et al. Nonphosphorylated tau slows down Aβ1–42 aggregation, binds to Aβ1–42 oligomers, and reduces Aβ1–42 toxicity. *J. Biol. Chem*. **296**, 100664 (2021).
42. Küffner, A. M. et al. Sequestration within biomolecular condensates inhibits Aβ-42 amyloid formation. *Chem. Sci.* **12**, 4373–4382 (2021).
43. Kanaan, N. M., Hamel, C., Grabinski, T. & Combs, B. Liquid-liquid phase separation induces pathogenic tau conformations in vitro. *Nat. Commun.* **11**, 2809 (2020).
44. King, M. R. et al. Macromolecular condensation organizes nucleolar sub-phases to set up a pH gradient. *Cell* **187**, 1889–1906.e24 (2024).
45. Lafontaine, D. L. J., Riback, J. A., Bascetin, R. & Brangwynne, C. P. The nucleolus as a multiphase liquid condensate. *Nat. Rev. Mol. Cell Biol.* **22**, 165–182 (2021).
46. Sanders, D. W. et al. Competing Protein-RNA Interaction Networks Control Multiphase Intracellular Organization. *Cell* **181**, 306–324.e28 (2020).
47. Yu, H. et al. HSP70 chaperones RNA-free TDP-43 into anisotropic intranuclear liquid spherical shells. *Science* **371**, eabb4309 (2021).
48. Rai, S. K., Khanna, R., Avni, A. & Mukhopadhyay, S. Heterotypic electrostatic interactions control complex phase separation of tau and prion into multiphasic condensates and co-aggregates. *Proc. Natl. Acad. Sci.* **120**, e2216338120 (2023).
49. Ye, S. et al. Micropolarity governs the structural organization of biomolecular condensates. *Nat. Chem. Biol.* **20**, 443–451 (2024).
50. Lu, T. & Spruijt, E. Multiphase Complex Coacervate Droplets. *J. Am. Chem. Soc.* **142**, 2905–2914 (2020).
51. Kaur, T. et al. Sequence-encoded and composition-dependent protein-RNA interactions control multiphasic condensate morphologies. *Nat. Commun.* **12**, 872 (2021).
52. Mountain, G. A. & Keating, C. D. Formation of Multiphase Complex Coacervates and Partitioning of Biomolecules within them. *Biomacromolecules* **21**, 630–640 (2020).
53. Lipiński, W. P. et al. Biomolecular condensates can both accelerate and suppress aggregation of α-synuclein. *Sci. Adv.* **8**, eabq6495 (2022).
54. Zhang, X. et al. The proline-rich domain promotes Tau liquid–liquid phase separation in cells. *J. Cell Biol.* **219**, e202006054 (2020).
55. Soeda, Y. et al. Intracellular tau fragment droplets serve as seeds for tau fibrils. *Structure* **32**, 1793–1807.e6 (2024).
56. Hurtle, B., Donnelly, C. J., Zhang, X. & Thathiah, A. Live-cell visualization of tau aggregation in human neurons. *Commun. Biol.* **7**, 1143 (2024).
57. Sinsky, J., Pichlerova, K. & Hanes, J. Tau Protein Interaction Partners and Their Roles in Alzheimer's Disease and Other Tauopathies. *Int. J. Mol. Sci.* **22**, 9207 (2021).
58. Siegert, A. et al. Interplay between tau and α-synuclein liquid–liquid phase separation. *Protein Sci. Publ. Protein Soc.* **30**, 1326–1336 (2021).
59. Kizhakkeduth, S. T. et al. Molecular Interactions between Tau Protein and TIA1: Distinguishing Physiological Condensates from Pathological Fibrils. *ACS Chem. Neurosci.* **7**, acschemneuro.4c00456 (2024).
60. Rai, S. K., Savastano, A., Singh, P., Mukhopadhyay, S. & Zweckstetter, M. Liquid–liquid phase separation of tau: From molecular biophysics to physiology and disease. *Protein Sci. Publ. Protein Soc.* **30**, 1294–1314 (2021).
61. Jacob, T. & Hoyer, W. Heterotypic phase separation in aggregation: Driver or deterrent? *Biophys. Chem.* **331**, 107577 (2026).
62. Gomes, L. A. et al. Aβ-induced acceleration of Alzheimer-related τ-pathology spreading and its association with prion protein. *Acta Neuropathol. (Berl.)* **138**, 913–941 (2019).

63. Koulouras, G. et al. EasyFRAP-web: a web-based tool for the analysis of fluorescence recovery after photobleaching data. *Nucleic Acids Res*. **46**, W467–W472 (2018).

Acknowledgements
We would like to acknowledge the Center for Advanced Imaging (CAi) at Heinrich Heine University for providing access to the Evident FV3000 Confocal Laser scanning Microscope (DFG-INST 1358/44-1 FUGB) and especially Sebastian Hänsch and Stefanie Weidtkamp-Peters for support during FRAP experiments and analysis.

Author contributions
T.J., M.P.S., G.T. and W.H. designed the experiments. T.J., M.P.S., L.G., L.H., G.L., G.T. and W.H. performed the experiments and analyzed the data. T.J. and W.H. wrote the manuscript. All authors commented on the manuscript.

Funding
W.H. discloses support for the research of this work from the European Research Council under the European Union's Horizon 2020 research and innovation program, grant agreement No. 726368. Open Access funding enabled and organized by Projekt DEAL.

Competing interests
The authors declare no competing interests.

Additional information
Supplementary information The online version contains supplementary material available at https://doi.org/10.1038/s42004-026-02165-6.

Correspondence and requests for materials should be addressed to Wolfgang Hoyer.

Peer review information *Communications Chemistry* thanks the anonymous reviewers for their contribution to the peer review of this work.